

# Analyzing 3D Limb Kinematics of *Drosophila Melanogaster* for Robotic Platform Development

Clarissa A. Goldsmith<sup>1(⋈)</sup>, Moritz Haustein<sup>2</sup>, Till Bockemühl<sup>2</sup>, Ansgar Büschges<sup>2</sup>, and Nicholas S. Szczecinski<sup>1</sup>

Department of Mechanical and Aerospace Engineering, West Virginia University, Morgantown, WV, USA clarissa@goldsmithgroup.org

<sup>2</sup> Institute of Zoology, University of Cologne, Cologne, Germany

**Abstract.** Recent work in insect-inspired robotics has highlighted the benefits of closely aligning the degrees of freedom (DoF) of a robotic platform with those of the target animal. However, to actualize this approach, the kinematics of the animal must be closely examined and balanced with considerations unique to a robotic counterpart. To inform the development of a robot inspired by *Drosophila melanogaster*, we collected 3D pose estimation data from the insect and analyzed the kinematics of the middle and hind limb pairs to find combinations of three DoF that best approximate animal motion. For our analysis, we simulated a baseline kinematic leg chain comprised of seven DoF for each frame of the motion capture data. We then fixed certain DoF and found a 'best fit' configuration relative to the animal. In these configurations, we analyzed the positional error of each joint's midpoints, as well as the angle of the leg plane from vertical. We found that using a three DoF combination of CTr elevation/depression, TrF pronation/supination, and FTi flexion/extension, we are able to closely approximate the motions of the insect while balancing necessary robotic platform considerations.

Keywords: Drosophila melanogaster · Drosophibot · Deep<br/>LabCut · Kinematic analysis

### 1 Introduction

In the context of legged locomotion, animals and robots can both be considered machines attempting to solve similar problems. In each case, a central controller dictates motor commands based on limb kinematics and dynamics and subject to modification from sensory feedback. While the consequences may vary, failure and success can be defined with similar criteria (e.g. remaining upright, making stable ground contact, adapting to dynamic terrain). Considering these criteria, animals currently have far greater walking capability than robots. However, the similarities between the two systems and their goals make it possible to

improve robotic walking capabilities through close investigation of animal locomotion. Many previous successful walking robots have been developed following this approach to varying degrees [10,12]. Additionally, a walking robot with a high degree of biological accuracy can be used as a test platform for biological hypotheses [3,4]. Such fidelity is key when using robots to investigate the animal nervous system, as the interplay between an organism's nervous system and mechanics is not presently understood. Highly bio-mimetic robots minimize controller-structure mismatch, ensuring greater neuroscientific applicability to data collected on the platform [9]. Such data can potentially be applied to more generic legged robot control, this continually expanding both fields.

Mimicking biology with a robotic platform presents challenges, however, such as actuation. While both animals and robots possess multi-jointed legs with actuators that control each joint, the design of robot legs is subject to different constraints than those of animals. Robotic systems are inherently limited by technological state-of-the-art, often a far cry from biological system capability. However, robot designs can be specialized in ways an animal's structure cannot without existential consequences. One common issue in this vein is muscles are considerably more compact and lightweight than conventional electric actuators, making it difficult to include all biological degrees of freedom (DoF) on a robotic counterpart without making the robot too heavy to stand. This constraint has often necessitated reducing the animal's various DoF to just three, the minimum DoF needed to position the chain's end effector at any arbitrary point in 3D space [14].

For certain groups of target animals, similar simplifications for leg DoF on robotic platforms have arisen over time. For example, many insect inspired robots follow a similar leg template of protraction/retraction with a thorax-coxa (ThC) joint, levation/depression with a coxa-trochanter (CTr) joint, and flexion/extension with a femur-tibia (FTi) joint [12]. Recently, however, Billeschou et al. highlighted the benefits of choosing specialized DoF based closely on the target animal's kinematics [3]. We wish to apply this methodology to our target animal, Drosophila melanogaster, in order to produce an updated version of our previous Drosophila inspired robot, Drosophibot, that more closely matches the animal's DoF [7].

In this work, we collect 3D pose estimation data from *Drosophila melanogaster* and conduct kinematic analysis on the middle and hind limb pairs to identify the three DoF that best approximate insect movement. We begin by constructing a simulated kinematic leg chain for each leg pair, then fix different DoF in the chain and attempt to construct a 'best fit' configuration to each frame of an animal data trial. We then investigate the effect these DoF fixations have on each joint's location in space and the angle of the leg plane to the vertical. In our analysis, fixing our hypothesized trochanter-femur (TrF) joint introduces high average error in the tip of the leg chain, as well as an inability to achieve animal-like leg plane angles. Meanwhile, fixing the ThC with a mobile TrF produces smaller positional error and maintains animal-like leg plane angles. We discuss the implications of these findings for understanding *Drosophila* leg kinematics, as well as our future goals to apply this analysis to the construction of a *Drosophila*-inspired robot.

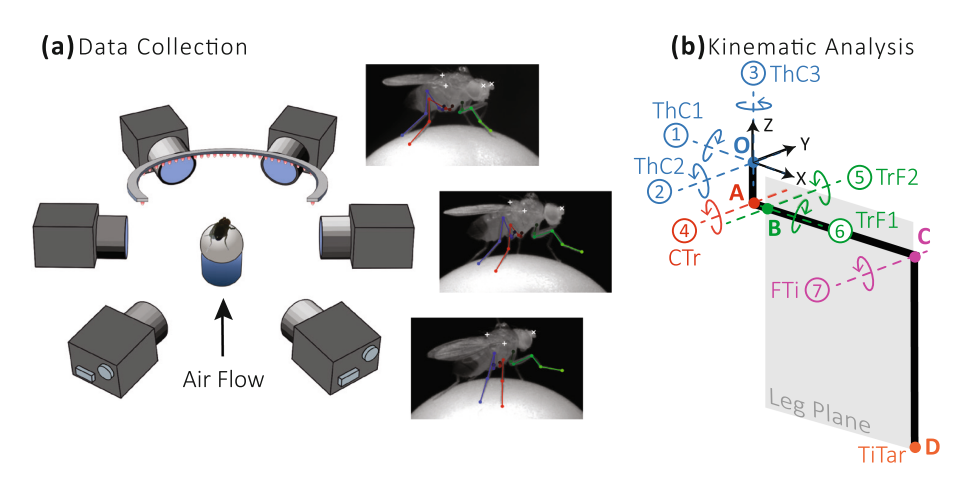


**Fig. 1.** (a) The spherical treadmill setup for acquiring 3D motion capture footage. (b) The DoF in our simulated leg chain, presented in the 'zero configuration' of the leg.

# 2 Methods

### 2.1 Data Collection

All experiments were performed with 3-to-8 days-old adult male and female Bolt-GAL4>UAS-CsChrimson *Drosophila melanogaster* flies [2]. This allowed optogenetic initiation of sustained, fast forward walking using a red laser (658·nm) targeting the animal's head. Animals were reared on a semi-synthetic agar standard medium soaked with 50  $\mu$ l of a 100 mmol L<sup>-1</sup> all-trans-Retinal solution at 25 °C and 65% humidity in the dark.

Tethered flies walked on a spherical treadmill [1] and leg movements were recorded with six synchronised high-speed cameras (Basler acA1300-200um with Kowa LM50JC1MS 50 mm lenses) surrounding the animal (Fig. 1a). Cameras were arranged such that either body side was recorded simultaneously by three cameras providing a front, side, and hind aspect. Videos were recorded 400 Hz and a resolution of 896 by 540 pixels. In each video, the flies stepped at frequencies between 5–13 Hz, corresponding to 30 to 80 postures per step cycle. We tracked the spatial position of six features on each leg: the thorax-coxa (ThC) joint, coxa-trochanter (CTr) joint, trochanter-femur (TrF) joint, femurtibia (FTi) joint, tibia-tarsus (TiTar) joint, and the tarsus tip. We also tracked the position of the posterior scutellum apex on the thorax, the wing hinge, and the antennae. Tracking was done automatically using the DeepLabCut toolbox [13], which we used to train three independent ResNet-50 networks (training sets: 630 frames for each network) for the front, side, and hind camera groups. Cameras were calibrated by using a custom-made checkerboard pattern  $(7 \times 6$ squares with size  $400 \,\mu\text{m} \times 400 \,\mu\text{m}$  per square). For triangulation of 3D feature positions, a singular value decomposition algorithm was applied [8]. 3D positions of the tracked features were transformed to a body-centered coordinate system derived from the triangle formed by the left and right wing hinge and the posterior scutellum apex.

# 2.2 Kinematic Analysis

The 3D animal position data was then used for kinematic analysis. For each leg, the animal data was normalized with the ThC as the origin of the leg's spatial frame. We only considered the middle and hind pairs of legs in our present work because the front limbs undergo considerably more complicated motions during walking.

Our analysis involved generating a simulated kinematic leg chain for every video frame, then attempting to find the 'best fit' configuration of the simulation to the animal data. We then repeated this analysis while fixing varying degrees of freedom (DoF) in the joints across a trial (i.e. an animal dataset). Our leg chain contains seven total DoF in the fully mobile case. Figure 1b shows the DoF of each joint in our 'zero configuration' for the leg. In the zero configuration, each DoF's axes of rotation are a direct translation of the spatial frame's axes: (1– 3) ThC protraction/retraction around the X axis (ThC1), levation/depression around the Y axis (ThC2), and rotation around the Z axis (ThC3); (4) CTr flexion/extension around the Y axis; (4-5) TrF flexion/extension around the X axis (TrF1) and rotation around the Y axis (TrF2); and (7) FTi flexion/extension around the Y axis [16]. The TiTar joint serves as the end effector of our leg chain. Historically, the TrF of *Drosophila* has been considered fixed [15]. However, findings of musculature and motor-neuronal innervation in the trochanter [5, 16], as well as the necessity of a 'CTr roll' in Lobato Ríos et al. 2021 [11] to most closely match animal kinematic replay raise questions regarding this claim, so we included a mobile TrF in our chain to test both cases.

Using this baseline leg structure, we created a function that uses product of exponentials to generate the simulated forward kinematic leg chain using the segment lengths for the present frame of animal data. Our calculation method uses the initial position of a point in the spatial frame,  $\vec{p}_{sim}(\vec{0})$ , as well as the deflection of each DoF from their zero configuration,  $\theta_1, \theta_2...\theta_7$ , to calculate the updated position of the joint in the spatial frame,  $\vec{p}_{sim}(\vec{\theta})$  [14]:

$$\vec{p}_{sim}(\vec{\theta}) = e^{\hat{\zeta}_1 \theta_1} e^{\hat{\zeta}_2 \theta_2} \dots e^{\hat{\zeta}_7 \theta_7} \vec{p}_{sim}(\vec{0}) \tag{1}$$

Each exponential term in Eq. 1 describes the twist of a single DoF's joint axes in space dictated by the frame's twist matrix,  $\hat{\zeta}$ :

$$e^{\hat{\zeta}\theta} = \begin{bmatrix} e^{\hat{\omega}\theta} & (I - e^{\hat{\omega}\theta})\hat{\omega}\vec{v} + \vec{\omega}\vec{\omega}^T\vec{v}\theta \\ 0 & 1 \end{bmatrix}, \tag{2}$$

where  $\hat{\omega}$  is the skew-symmetric matrix of the DoF axis of rotation,  $\vec{\omega}$ , and  $\vec{v}$  is the zero-configuration location of the DoF frame's origin in the spatial frame.

We then embedded  $\vec{p}_{sim}(\vec{\theta})$  in an error function for the  $i^{th}$  joint,  $e_i(\vec{\theta})$ :

$$e_i(\vec{\theta}) = \frac{w_i}{l_i} \|\vec{p}_{sim,i}(\vec{\theta}) - \vec{p}_{fly,i}\|. \tag{3}$$

This function calculates the magnitude of the error between the simulated position of a joint (labeled A–D in Fig. 1) for a certain vector of joint angles,  $\vec{p}_{sim,i}(\vec{\theta})$ , and the point position from the animal,  $\vec{p}_{fly,i}$ , normalized by the length of the joint's proximal leg segment,  $l_i$ , and scaled by a weighting,  $w_i$ . Segment lengths are re-calculated from the animal data for each frame in order to minimize the effect of point tracking errors on the positional error between animal and simulated leg chains. We prioritized fit toward the end of the chain in our simulations by setting the weights  $w_A, w_B, w_D = 1$  and  $w_C = 3$ .

Each of these error functions were then combined into an error vector,  $\vec{E}(\vec{\theta})$ . For each frame of the target leg's positional data, we minimized the vector norm of  $E(\vec{\theta})$  to construct a 'best fit' configuration of our simulated leg with the least overall euclidean distance of each tracked point to the animal points. The fixed joint's angles were set as constants based on their average value in the fully mobile case. Once we found the best fit configuration, we stored the unweighted positional errors normalized to each joint's proximal segment. We also calculated the angle of the leg plane, a plane containing the femur and tibia (grey plane in Fig. 1b), from the vertical for both the animal and simulation. This process was repeated for every frame of a trial.

For choosing joint fixations, we primarily focused on the ThC and the TrF. The CTr and FTi have proven innervation and noticeable angular movement during stepping, so they were left mobile in all cases [15,16]. The ThC has similar evidence, but the difficulty of creating an electrically actuated 3 DoF joint at our scale motivated us to attempt to eliminate ThC DoF if possible. As the mobility of the TrF is presently debated, fixing TrF DoF also proved a natural choice.

# 3 Results

Figures 2 and 3 show the average spatial error over each trial of each of the simulated limb pairs' joints compared to the animal data for five different leg 'structures': 'all joints mobile', 'ThC1, ThC2 fixed', 'ThC1, ThC2, TrF2 fixed', 'ThC Fully Fixed, TrF2 Fixed', and 'ThC1, ThC2 Fixed, TrF Fully Fixed'. In the error plots, each symbol and color combination represents a different fly. Of the pair, the filled symbol represents the fly's right limb, and the unfilled symbol the left limb. Because we normalized the errors of each point to the length of the proximal segment, the average values are presented as a fraction of the proximal segment's length.

In the 'all joints mobile' case for the middle legs (Fig. 2a), the errors in the FTi and TiTar positions are relatively small, signifying a good match to the animal's foot trajectories. The errors for the CTr and TrF spatial position are slightly higher (nearly 0.1 coxa lengths of average CTr error), likely due to

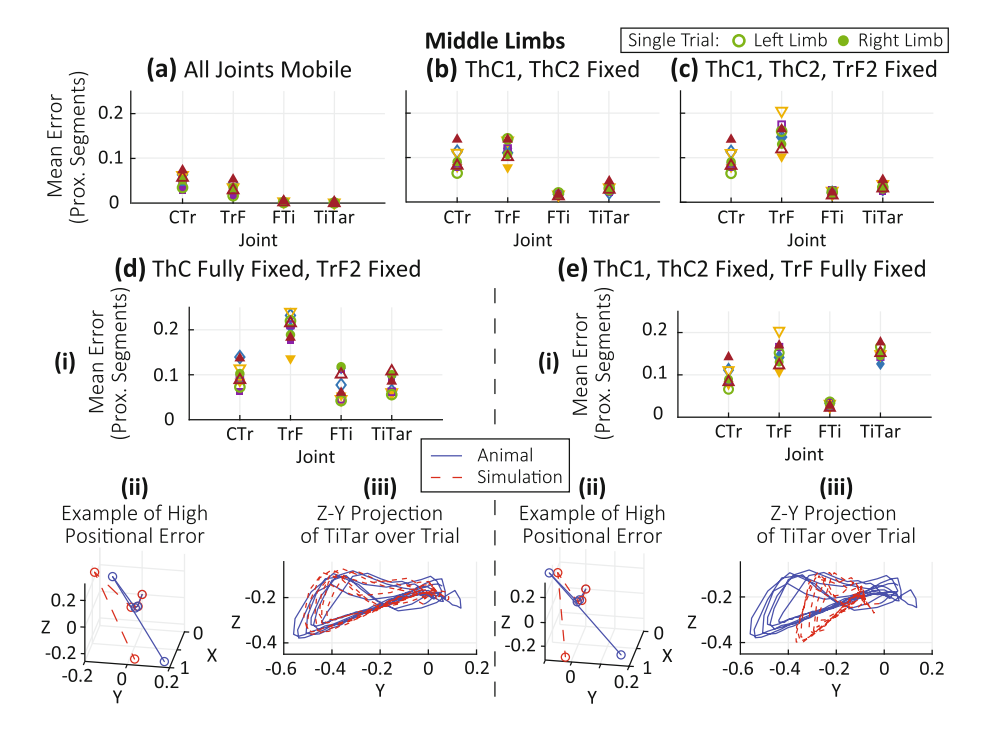


Fig. 2. Fixing TrF rotation greatly impacts the middle leg's ability to capture animal-like positions of tracked points on the animal. Each symbol/color represents a different fly. A filled symbol represents a right limb, an unfilled symbol a left limb. The error is normalized in terms of a fraction of the joint's proximal segment length. The mean normalized errors in the middle limbs are plotted for: (a) all joints mobile; (b) the ThC1 and ThC2 fixed; (c) the ThC1, ThC2, and TrF2 fixed; (di) the ThC fully fixed and the TrF2 fixed; and (ei) the ThC1 and ThC2 fixed and the TrF fully fixed. The leg chains for the animal (solid blue) and the simulation (dashed red) are plotted for the latter two cases (dii, eii) in a frame of high error, as well as the Z-Y projection of the TiTar over a single trial (diii, eiii). (Color figure online)

motion capture artifacts and video resolution limitations making it harder to pinpoint joint locations close to the thorax. Additionally, because the coxa and trochanter are relatively short segments in the limb, the error is inflated by our normalization. As seen in dii and eii of Fig. 2, these errors do not end up creating significant positional deviations from the animal data.

When the ThC1 and ThC2 are fixed in the middle limbs as in Fig. 2b, the average error in each segment slightly increases. However, the error at the end of the leg chain still remains low. This trend continues as we additionally fix the TrF2 (Fig. 2c).

Fixing the ThC3 to fully fix the ThC, in contrast, greatly increases average FTi and TiTar joint point error in the middle limbs (Fig. 2di). In this case, the FTi and TiTar points experience errors 2–5 times larger than the errors

from the previous case in Fig. 2c. Figure 2dii shows the animal and simulation leg chains during a frame of high positional error to highlight this discrepancy. During such frames, the FTi and TiTar points do not fully match the positions of the animal data. However, the leg does achieve a similar angle of the leg plane. Additionally, the Z-Y projection of the simulated limb's TiTar position over the trial (red dashed line, Fig. 2diii) is still able to follow a similar path as the animal's. The major discrepancies occur at the transitional periods between leg stance and swing.

Fully fixing the TrF and mobilizing the ThC3 (Fig. 2e), by contrast, produces a more drastic effect. As shown in Fig. 2ei, fixing the TrF1 decreased the average error of the FTi point from the ThC3-fixed case, but also greatly increased the average error of the TiTar point. Looking at a frame of high error (Fig. 2eii), the simulated limb chain more accurately captures the FTi joint point than with the ThC3 fixed. However, the simulated leg plane's angle deviates greatly from the animal's, causing large TiTar point error. This error causes large discrepancies in the trajectories of the TiTar point projected on the Z-Y plane between animal and simulation (Fig. 2eiii). Overall, completely fixing the TrF joint in the middle limbs greatly diminished our simulation's ability to accurately capture the limb movements of the animal.

Analysis of the hind legs revealed similar patterns as in the middle legs (Fig. 3). The fit of the hind limb with all joints mobile (Fig. 3a) had similar errors as the middle limb, which we attributed to resolution limitations and motion capture artifacts. The hind limbs also showed minimal increase in end effector error when fixing the ThC1, ThC2, and TrF2 (Fig. 3b–c). Fully fixing the ThC (Fig. 3di) resulted in increased error for all points, particularly in the FTi and TiTar. The leg chains in a position of high error in Fig. 3dii show a similar behavior as the middle limbs in this case: the simulated FTi and TiTar are not able to achieve the same positioning as the animal, but the overall angle of the leg plane appears similar. The simulated hind limb is also able to complete a similar TiTar Z-Y trajectory as the animal, albeit with less overall protraction and retraction (Fig. 3diii).

The major difference between the middle and hind limb behavior appears when the TrF is fully fixed and the ThC3 is made mobile (Fig. 3e). The average error of the FTi and TiTar points both decrease (Fig. 3ei), signifying an improved fit. Plotting the leg chains supports this idea (Fig. 3eii); the simulated limb is still not fully able to achieve the position of the animal data, but the spatial distance between the two chains is shorter. The position of the TiTar over time further shows a closer fit between the two datasets (Fig. 3eiii).

To further elucidate the differences between fully fixing the ThC vs. the TrF, we also calculated the angle of the leg plane from vertical, shown in Fig. 3. Similar to the error plots, fixing the ThC1, ThC2, and TrF2 in (a–c) causes minimal increases («5 °C in most cases) in the angle errors (Fig. 3a). The range of leg plane angles over the trial also remains similar (Fig. 3b).

The angle data for combinations (d–e) in the middle limb also seems to align with the error data. The highest average angle error occurs when the TrF is fully

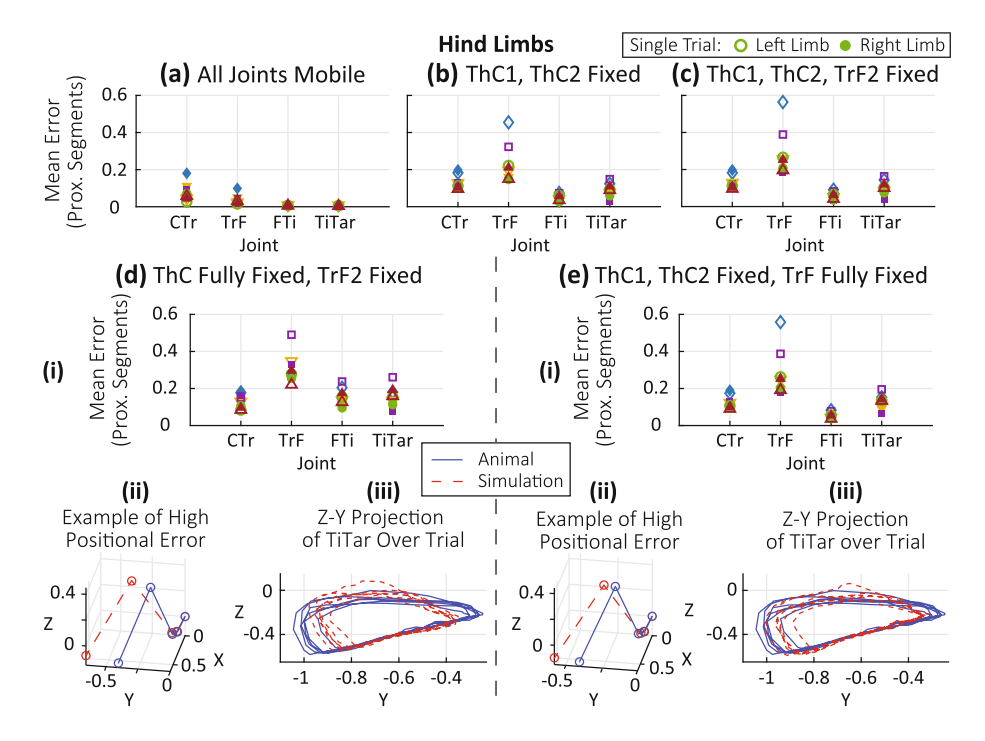


Fig. 3. Fixing the ThC3 or the TrF1 in the hind limbs does not produce as stark of a difference in point positional error as fixing them in the middle limbs. Each symbol/color represents a different fly. A filled symbol represents a right limb, an unfilled symbol a left limb. The error is normalized in terms of a fraction of the joint's proximal segment length. The mean normalized errors are plotted for: (a) all joints mobile; (b) the ThC1 and ThC2 fixed; (c) the ThC1, ThC2, and TrF2 fixed; (di) the ThC fully fixed and the TrF2 fixed; and (ei) the ThC1 and ThC2 fixed and the TrF fully fixed. The leg chains for the animal (solid blue) and the simulation (dashed red) are plotted for the latter two cases (dii, eii) in a frame of high error, as well as the Z-Y projection of the TiTar over a single trial (diii, eiii). (Color figure online)

fixed, as shown in Fig. 3ai. The total range of angles is also much lower with the TrF fixed (Fig. 3bi). The ThC being fully fixed, meanwhile, produces less average error and a much closer range of angles over the trials. Figure 3ci, showing typical angles over a trial, highlights the difference between the two ranges. While fully fixing the ThC causes the simulation (red dashed line) to overshoot the animal's (blue solid line) peak angles slightly, the overall waveform follows the animal's. With the TrF fixed, however, the simulated leg is unable to achieve angles close to those of the animal.

The data in Fig. 3 also helps elucidate the key DoF in the hind limbs. Figure 3aii shows that the average leg plane angle error is highest with the ThC fully fixed. With the ThC3 mobile instead, the error shifts closer to baseline levels. Fully fixing the ThC also produces much higher angle ranges (Fig. 3bii),

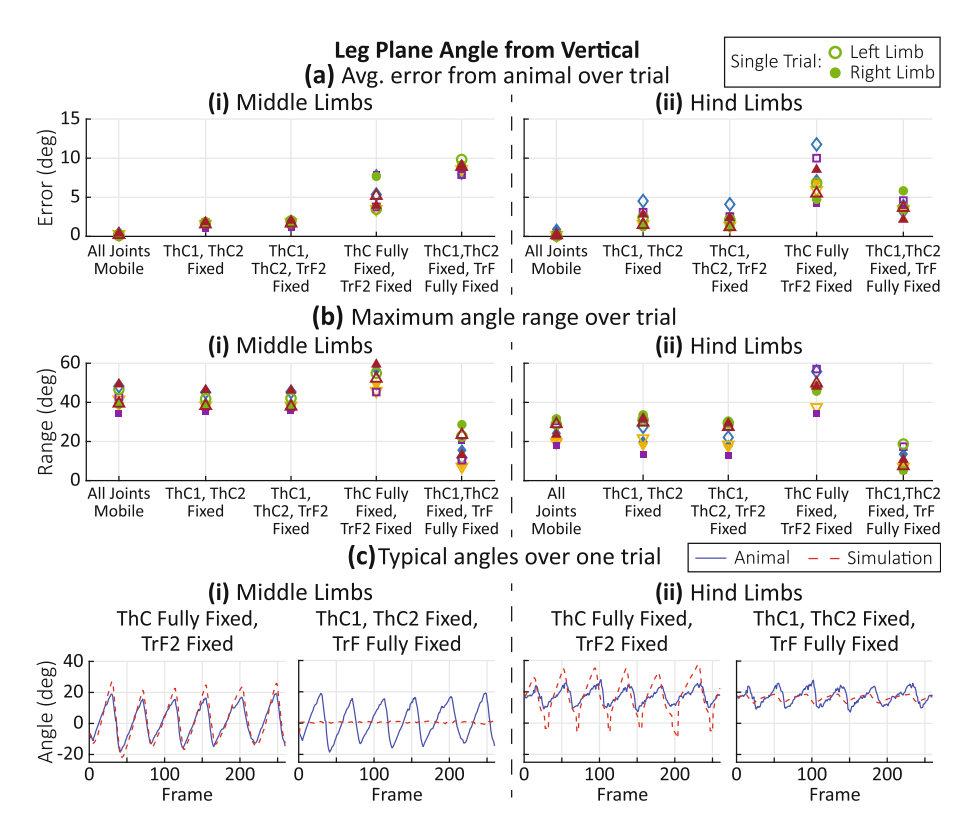


Fig. 4. Investigating tibia angles from vertical for various limb structures helps further illuminate movement differences. Each symbol/color represents a different fly. A filled symbol represents a right limb, an unfilled symbol a left limb. (a) The average error between the simulation and the animal over a trial for the middle (i) and hind (ii) limbs for various DoF structures. (b) The maximum range of angles over a trial for the simulated middle (i) and hind (ii) limbs. (c) Typical angles over a trial for the animal (blue solid) and simulation (red dashed) while the ThC and TrF2 were fixed, and the TrF, ThC1, and ThC2 were fixed. Data is included in both configurations for the middle (i) and hind (ii) limbs. (Color figure online)

similar to the middle limbs. However, the baseline range for the hind limbs is about half that of the middle limbs, so the higher ranges cause an increased overall error. Figure 3cii highlights how the modified ranges affect the fit to the animal data over a trial (Fig. 4).

# 4 Discussion

In this work, we analyzed the kinematics of the middle and hind limbs of *Drosophila melanogaster* from 3D pose estimation data, with the aim of determining the three most crucial degrees of freedom (DoF) to include on the corresponding limbs of a fruit fly inspired robot. We constructed a kinematic chain of

the limb for each frame of the data and attempted to determine a 'best-fit' configuration to the animal data. This process was repeated over an entire animal trial with different DoF fixed. Our kinematic chain was based on five reported DoF in *Drosophila* [15,16], as well as a mobile TrF joint with two DoF. Our findings show that with our chosen DoF orientations, fixing the ThC1, ThC2, and TrF2 joints created minimal error between the simulation and the animal. Fixing either the ThC3 or TrF1 joints, both of which provide a pronation/supination motion, created much larger errors throughout the leg chain, particularly toward the end effector. For the middle limbs, fully fixing the TrF left the simulated leg unable to match the angle of the leg plane from the vertical found in the animal. Meanwhile, fixing the ThC fully retained the leg's ability to achieve animal-like angles. For the hind limbs, fixing these joints had similar results, but due to the smaller range of leg plane angles in the animal's hind limbs, fixing the TrF produced a slightly closer match.

Using these results, we made a final determination about the limbs of our updated *Drosophila* robot. For both limb pairs, the low errors produced by the fixation of the ThC1, ThC2, and TrF2 joints allow us to omit them entirely from the leg designs. Similarly, the high degree of both positional and angular error produced in the middle limbs upon fully fixing the TrF leads us to include the TrF1 joint over the ThC3. Thus, we will include the CTr, TrF1, and FTi joints as the three DoF in our robotic middle limb.

The hind leg pair presents a less straightforward decision. Based on the leg plane angle data shown in Fig. 3, fixing the TrF1 in conjunction with the ThC1, ThC2, and TrF2 provides the least angular error. However, the increased range of leg plane angles when fixing the ThC3 could be uniquely beneficial to a robotic platform. In stance phase, an organism's body weight produces a vertical ground reaction force (GRF) at the foot, producing moments in the frontal plane on the proximal end of each leg segment. Components of these moments aligned with the joint axis must be counteracted by the actuator, while the rest are passively resisted by the joint structure. Thus, a larger leg plane angle results in lower actuator torques than a vertical plane. Billeschou et al. demonstrated as such by creating an angle in the leg planes of their dung beetle robot, which better distributed the torques required to support the body among all the actuators of the leg [3]. Zill et al. similarly found that the force profiles encoded by the stick insect's trochanteral campaniform sensilla were highly dependent on the orientation of the leg plane [17]. This redistribution of torque could provide a further factor of safety for our robot. Additionally, it is presently unclear how the hind limb motions are affected by walking on a curved surface vs. a flat surface. As shown in Figs. 2d and 3d, during stance the hind TiTar moves along a path approx. twice as steep as the middle TiTar. As such, hind limb motions may be more similar to the middle limbs on flat ground. For these reasons we conclude that including the CTr, TrF1, and FTi joints in our robot's hind limbs is most beneficial to our present purposes.

We found it curious that with our investigated DoF we could not achieve animal-like limb movements without a mobile TrF, despite no conclusive evidence of the joint's mobility in *Drosophila*. Other *Drosophila* studies have found similar results: adding 'CTr roll' decreased kinematic replay error in Lobato Ríos et al. 2021, creating pronation/supination motion added similar to our TrF [11]. Studies of larger species within *Diptera* during flight have reported pronation/supination in the CTr of the unloaded middle limbs [6]; however, this joint movement has not been observed during loaded walking. No final determination can be made about this pronation/supination or the mobility of the TrF in *Drosophila* without the identification of condyles or specific neuronal innervation. However, we believe our data contributes to a growing call to more closely examine the mobility of *Drosophila*'s legs.

Our work presently targets only a small subset of fly leg behaviors. In addition to forward walking, flies can walk in curves, walk backward, and turn in place, in addition to behaviors such as searching, cleaning, mating, etc. The apparent overactuation of insect legs could serve the need to perform such varying functions. It is unclear how well our proposed simplified leg structures can emulate non-walking movements, but such behaviors are outside of our present scope. We plan to apply our present methodology to omni-directional walking in future work.

We also do not address the tarsal segment of *Drosophila*, a common simplification for insect-inspired robots. However, biologically the tarsus comprises a large portion of the leg length and plays an important role in managing ground interactions [12]. We aim to further explore the role of the tarsal segment in future work.

For robot design, our future work will first involve analysis of the fly's front limbs. We believe our present methodology can be directly applied, though more than three DoF will likely be needed to capture the greater movement complexity. We will then conduct dynamical analysis of the proposed robot design through a dynamic simulation of the robot. The simulation will allow us to test leg movements corresponding to forward, backward, and curved walking on a flat surface in lieu of biological motion capture. We will use the calculated forces and torques to inform final mechatronic design (e.g. actuator selection). With the resulting robot, we seek to expand our work developing synthetic nervous system controllers like the controller developed for our previous robot, Drosophibot [7]. We also plan to explore how the campaniform sensilla discharge in insect limbs is influenced by leg movements [18].

**Acknowledgements.** Many thanks to Sasha Zill for his comments and insight while preparing this manuscript. This work was supported by NSF DBI 2015317 as part of the NSF/CIHR/DFG/FRQ/UKRI-MRC Next Generation Networks for Neuroscience Program.

# References

- Berendes, V., Zill, S.N., Büschges, A., Bockemühl, T.: Speed-dependent interplay between local pattern-generating activity and sensory signals during walking in Drosophila. J. Exp. Biol. 219(23), 3781–3793 (2016)
- Bidaye, S.S., et al.: Two brain pathways initiate distinct forward walking programs in Drosophila. Neuron 108, 469–485 (2020)
- 3. Billeschou, P., Bijma, N.N., Larsen, L.B., Gorb, S.N., Larsen, J.C., Manoonpong, P.: Framework for developing bio-inspired morphologies for walking robots. Appl. Sci. 10(19), 6986 (2020)
- Buschmann, T., Ewald, A., von Twickel, A., Büschges, A.: Controlling legs for locomotion-insights from robotics and neurobiology. Bioinspir. Biomim. 10(4), 41001 (2015)
- Enriquez, J., Venkatasubramanian, L., Baek, M., Peterson, M., Aghayeva, U., Mann, R.: Specification of individual adult motor neuron morphologies by combinatorial transcription factor codes. Neuron 86(4), 955–970 (2015)
- Frantsevich, L.: Biomechanics of the multisclerite middle coxa in flies (Diptera).
  Arthropod Struct. Dev. 29(2), 147–161 (2000)
- Goldsmith, C.A., Szczecinski, N.S., Quinn, R.D.: Neurodynamic modeling of the fruit fly Drosophila melanogaster. Bioinspir. Biomim. 15, 065003 (2020)
- Hartley, R.I., Zisserman, A.: Multiple View Geometry in Computer Vision, 2nd edn. Cambridge University Press, Cambridge (2003)
- Hooper, S.L.: Body size and the neural control of movement. Curr. Biol. 22(9), R318–R322 (2012)
- Ijspeert, A.J.: Biorobotics: using robots to emulate and investigate agile locomotion. Science 346(6206), 196–203 (2014)
- Lobato Ríos, V., et al.: NeuroMechFly, a neuromechanical model of adult Drosophila melanogaster. bioRxiv (2021). https://doi.org/10.1101/2021.04.17. 440214
- Manoonpong, P., et al.: Insect-inspired robots: bridging biological and artificial systems. Sensors 21(22), 1–44 (2021)
- Mathis, A., et al.: DeepLabCut: markerless pose estimation of user-defined body parts with deep learning. Nat. Neurosci. 21(9), 1281–1289 (2018)
- 14. Murray, R., Li, Z., Sastry, S.: A Mathematical Introduction to Robotic Manipulation, 1st edn. CRC Press, Boca Raton (2017)
- Sink, H.: Muscle Development in Drosophila, 1st edn. Springer, New York (2006). https://doi.org/10.1007/0-387-32963-3
- Soler, C., Daczewska, M., Da Ponte, J.P., Dastugue, B., Jagla, K.: Coordinated development of muscles and tendons of the Drosophila leg. Development 131(24), 6041–6051 (2004)
- Zill, S.N., Schmitz, J., Chaudhry, S., Büschges, A.: Force encoding in stick insect legs delineates a reference frame for motor control. J. Neurophysiol. 108(5), 1453– 1472 (2012)
- Zyhowski, W., Zill, S., Szczecinski, N.: Load feedback from a dynamically scaled robotic model of Carausius Morosus middle leg. In: Verschure, M. (ed.) Living Machines 2022. LNAI, vol. 13548, pp. 128–139. Springer, Cham (2022)